Pergamon

Int. J. Solids Structures Vol. 32, No. 19, pp. 2923–2943, 1995
Elsevier Science Ltd
Printed in Great Britain

0020–7683(94)00237–1

CONCERTINA TEARING OF METAL PLATES

TOMASZ WIERZBICKI
Department of Ocean Engineering, Massachusetts Institute of Technology, Cambridge, MA 02139, U.S.A.

(*Received* 5 *April* 1994; *in revised form* 16 *September* 1994)

Abstract—Small scale experiments on wedge indentation into metal plates revealed the existence of two different failure modes. In the case of sharp wedges with a small tip angle, plates failed by developing a longitudinal cut at or ahead of the tip of the wedge followed by the formation of two curls at the wake of the wedge. However, the same plates failed by folding in front of the wedge and tearing at remote boundaries when the wedge was blunt and/or the tip angle was large. This so-called "concertina tearing" mode was also observed in intermediate scale laboratory tests and in real-world grounding accidents. The present paper develops a simplified theory of the process of concertina tearing. Closed-form solutions are derived for the plate-resisting force and the length of the folding wave. The results were compared with small and intermediate scale indentation tests on metal plates, and showed good agreement.

1. INTRODUCTION

Vaughan (1979) and Jones and Jouri (1987) performed a series of impact indentation tests on metal plates using a drop tower facility. Quasi-static wedge indentation tests using a universal testing machine were described by Lu and Calladine (1990) and, more recently, by Thomas (1992). Typically, plates were positioned parallel to the motion of the wedge or were tilted by 10° or 20°. These experiments revealed the co-existence of two different failure modes of plates. Depending on wedge geometry, a longitudinal cut was developed ahead or at the tip of the wedge. The flaps in the wake of the wedge curled into two approximately cylindrical surfaces (Fig. 1). However, some of the plates did not follow the above failure pattern even though the wedge cutting edge was sharp and plates were pre-cut to facilitate fracture initiation. Instead, the plate material piled up in front of the wedge and tore at some remote location, typically at the clamped longitudinal edges of the plate (Fig. 2). If continued, the process left a torn-off and folded strip of the plate, much resembling a "concertina" folding mode.

Initially, the appearance of the concertina tearing mode was considered an unwelcome disturbance to the well-planned plate cutting experiments. However, in the light of additional evidence from small scale tests (Maxwell, 1993; Yahiaoui *et al.*, 1994), intermediate scale experiments (Paik, 1994), and large scale tests (Astrup, 1994; Kuroiwa *et al.*, 1992; Kitamura *et al.*, 1978), it became clear that concertina tearing is one of the common failure modes of plates subjected to in-plane indentation load. Such loads are typically developed when the bottom of a ship strikes a rock or reef in grounding accidents. Interestingly, concertina tearing was identified by the author in the photograph of a ground-damaged bottom of a supertanker. The portion of the hull plating between two longitudinal stiffeners was torn off and folded in an alternating wavy fashion and then pushed aside by the rock.

The objective of the present paper is to report on the development of a simple computational model of the process of steady concertina tearing. The present theoretical predictions are compared with experimental results and give consistently good correlations.

2. DESCRIPTION OF TESTS

Three types of tests were conducted in a screw-driven universal testing machine with a long stroke. In all cases, a thin metal plate was mounted in a heavy U-shaped frame. The

plate was secured to the frame by a row of bolts and specially-designed drawbids to prevent in-plane slippage.

In the first type of test, a wide wedge ($2\theta = 60^\circ$) was pressed with tilt angles of 0°, 10° and 20°. Unless the plate was pre-cut at the center, the failure almost inevitably initiated at the clamped boundary and consisted of a pair of longitudinal tears with an alternating folding of the plate. A photograph of a typical damaged plate in this failure mode is shown in Fig. 2. The corresponding force–displacement relationship recorded in the test is plotted in Fig. 3. It should be noted that concertina tearing persisted even for a relatively large tilt angle, $\alpha = 20^\circ$. A detailed description of the above tests was given by Maxwell (1993).

In the second type of test, concertina tearing was induced in long and narrow plates. The damaged zone was confined to a narrow strip of a larger plate, between two longitudinal stiffeners welded to the plate at a distance b apart. When the width to thickness ratio b/t was in the range 30–60, an extremely regular folding pattern was observed (Fig. 4). The folded plate piled up in front of the wedge in a stable fashion, meaning that the cracks at both edges of the plate strip were advancing at approximately the same speed and that no loss of lateral stability of the crushed portion of the plate occurred at the maximum cross-head travel distance of 350 mm.

In many ways, the process of concertina tearing is similar to the process of concertina crushing of circular and rectangular tubes (Alexander, 1960; Wierzbicki *et al.*, 1992). In both cases, the damage process is progressive, and each peak and valley in the load–deformation curve corresponds to the formation of one distinct folding wave with a characteristic length of $2H$. An interesting feature of the concertina tearing is that, once initiated, the deformation process is independent of the shape and size of the wedge (semi-angle, θ, tip radius) and friction between the wedge and the plate. This is explained by the fact that the material is piling up in front of the wedge, and plastic flow and fracture occur at remote locations with respect to the wedge tip. For a detailed description of the test program, the reader is referred to the work of Yahiaoui *et al.* (1994). In the third type of test, with narrow wedges tearing wide or infinite plates, still another failure mode was identified. This mode in which two diverging cracks develop from a suitable initial pre-cut is shown in Figs 5a and 6.

The present paper is concerned with the analysis of the type of concertina tearing where two parallel cracks proceed along the clamped longitudinal edges of the plate (Fig. 5b). The latter case, in which the shape of the diverging crack trajectories is an additional unknown of the solution, is studied in a separate publication (Wierzbicki and Trauth, 1994).

3. DEVELOPMENT OF A SIMPLIFIED FAILURE MODE

Consider a plate of width b and thickness t. The plate is firmly clamped along the parallel edges and is loaded by a punch or wedge slowly advancing with a velocity $\dot{u}$. The wedge is modelled as a point load F applied at the mid-span. As mentioned before, the geometry of the wedge, usually described by its semi-angle θ, width B and tip radius r, does not enter the solution because the material folds and piles up in front of the wedge. Except for the initiation stage of the cutting process, the solution for the total resisting force is independent of the geometry of the wedge or punch.

Because of similarities in the process of concertina tearing and concertina folding of tubes, the present modeling concept will draw heavily from the experience gained in solving the problem of axial crushing of circular and rectangular columns. It was shown by Alexander (1960), Wierzbicki and Abramowicz (1983), and Wierzbicki and Huang (1991) that accurate results are obtained by considering geometrically compatible folding mechanisms with plastic deformations localized in generalized plastic hinge lines and rigidly displacing and rotating plate elements. The plastic work dissipated in bending, compression/tension and in-plane shear is concentrated in the generalized hinge lines. At first glance, the final deformation pattern of the plate suggests that the tearing process proceeds in an out-of-plane mode III fracture. However, a close examination of the sequential failure process in many test pieces has revealed that a true tearing failure is a combination of all

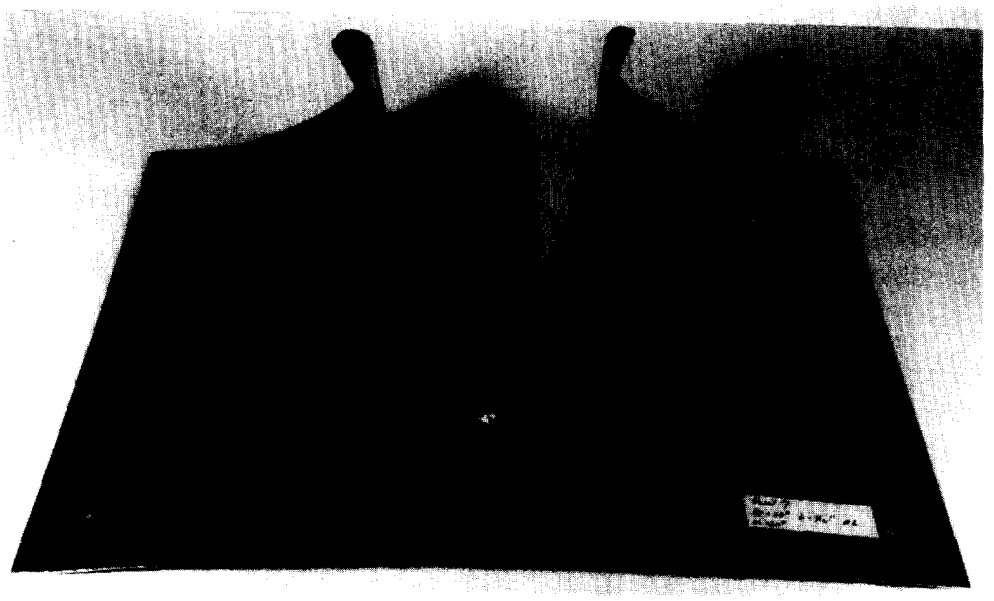

Fig. 1. A typical deformation pattern in a clean cut and curl mode of a plate by a wedge.

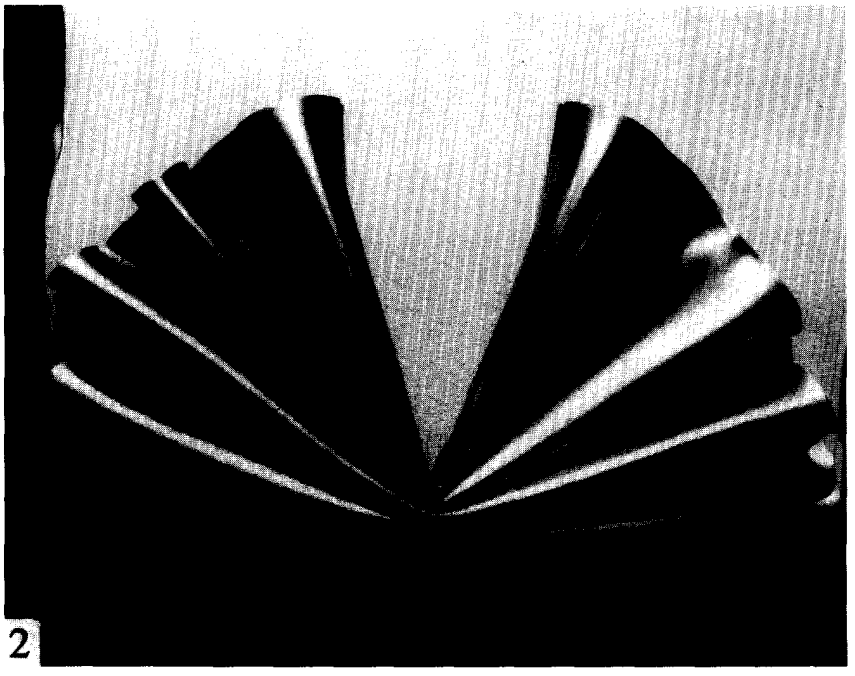

Fig. 2. A photograph of a typical concertina tearing failure mode of a wide plate.

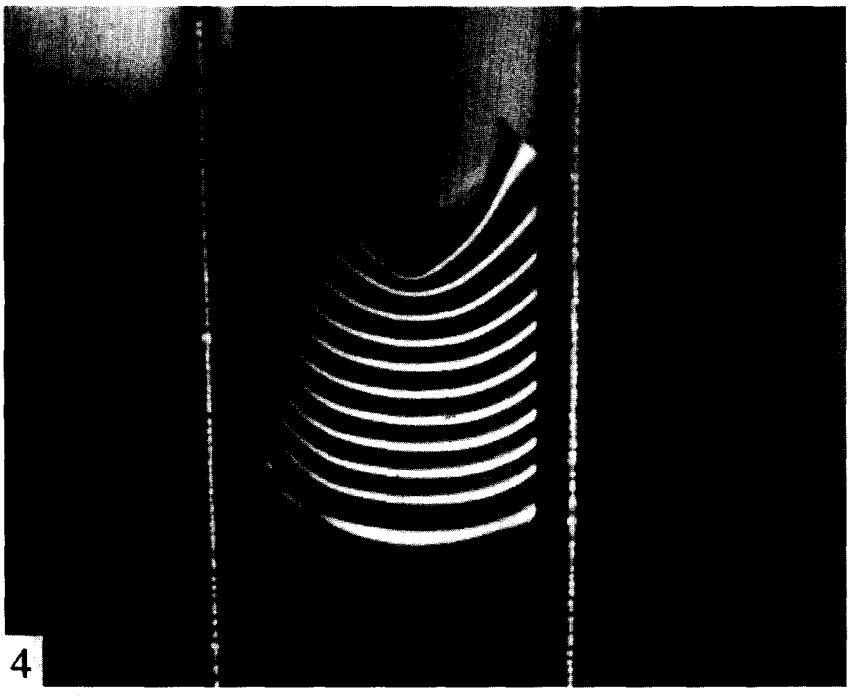

Fig. 4. A fully developed regular concertina tearing mode of a narrow plate.

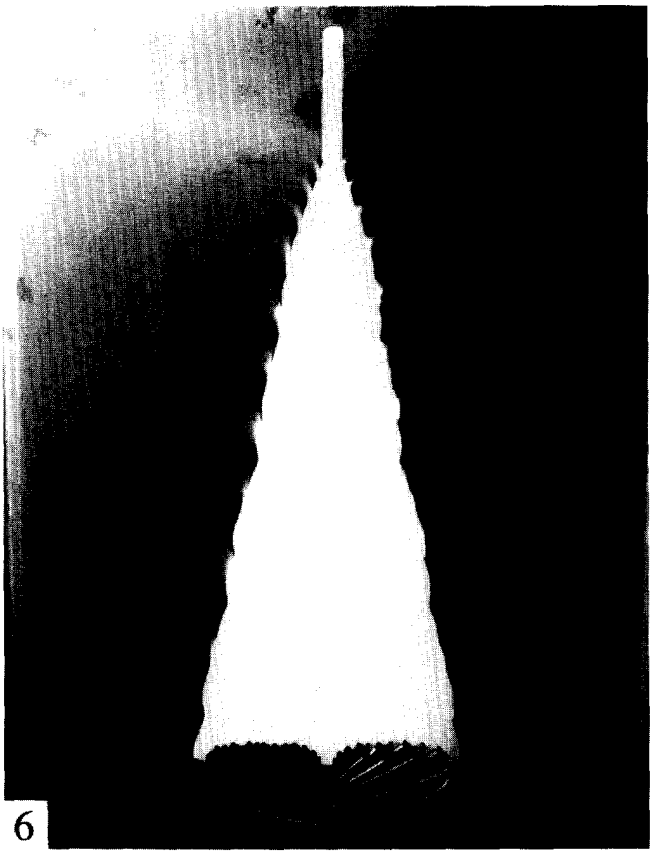

Fig. 6. A concertina tearing mode with two diverging cracks originating from a local cut.

Fig. 12. Concertina tearing of the plate by a round wedge.

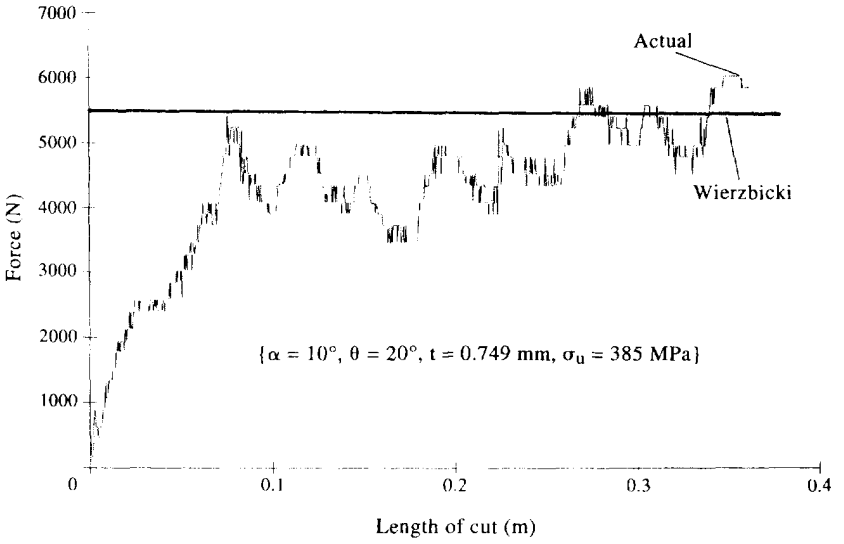

Fig. 3. A load–displacement diagram of the plate shown in Fig. 2. Each local peak corresponds to the formation of one folding wave.

three fracture modes, with the in-plane mode I fracture being dominant. The present computational model must thus capture a simultaneous in-plane tearing and out-of-plane folding of a given plate element.

In the past, models of progressive folding of tubes have been constructed in which one fold is formed at a time (Alexander, 1960; Wierzbicki and Huang, 1991). A distinctive feature of concertina tearing is that in order to achieve full geometric compatibility, two active folds must interact at all times. Therefore, formation of a full fold consists of two phases. Because of this periodic nature of the process of concertina tearing, the plate can be divided by equally spaced lines into narrow plate elements of length H (H is the half length of the plastic folding wave), yet to be determined (Fig. 7).

In the first phase, a "roof"-type mechanism is formed with stationary hinge lines and zones of in-plane compression in the transverse direction (Figs 7 and 8). Two diagonal hinge lines DG and NG appear on both sides of the plate and meet at an unknown distance ξ from the support. With the parameters H and ξ fixed for the entire process, the model represents a one-degree-of-freedom mechanism. As the leading edge BC of the plate (which is in contact with the wedge) advances, the front rectangular element BCGF and the back trapezoidal panel (KFGNML) rotate in the out-of-plane direction by an angle θ. At the same time, the two triangular elements (DGN) rotate in both the out-of-plane and the in-plane directions. This causes tearing fracture at the support and compression/tension deformation in the front trapezoidal panel. The amount of compression is represented in Fig. 7 by two shaded triangles with an overlap Δ. The first phase terminates when the back trapezoidal element and the central rectangular element BCGF assume a vertical position and first touching occurs. At this time, the tearing process of the edges DN and AK terminates over the entire length $2H$.

In the second phase, new hinge lines are formed at the center of triangular elements EF and GI and across the back trapezoidal element GM and FL. As the lines BC and LM (now contiguous) advance into new material, the tearing process halts. Bending continues along newly formed hinge lines while the diagonal hinge lines undergo re-bending (Fig. 8c). Note that the length of the line KLMN remains unchanged while the corresponding length A′B′C′D′ of the next element is being shortened by the amount 2Δ (shaded area). Clearly, there must be a shear deformation at the interface between the neighboring elements. The second phase terminates when points A and D meet respectively with points K and N. All plate elements assume a vertical position and the central portion of the element penetrates a full distance $2H$ into the new element (Fig. 9).

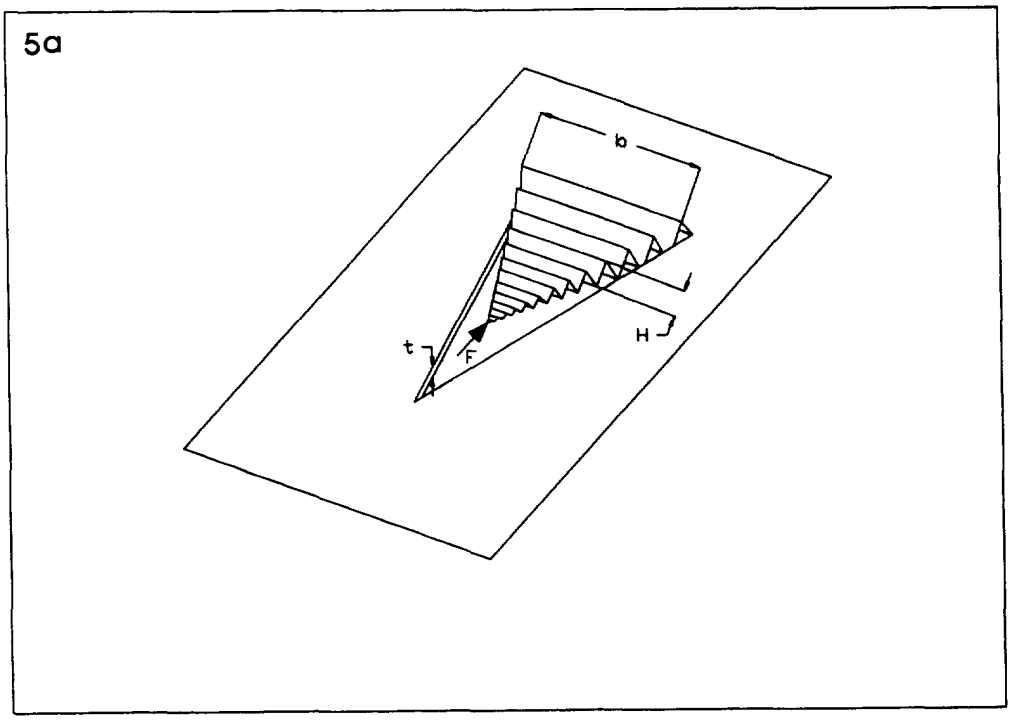

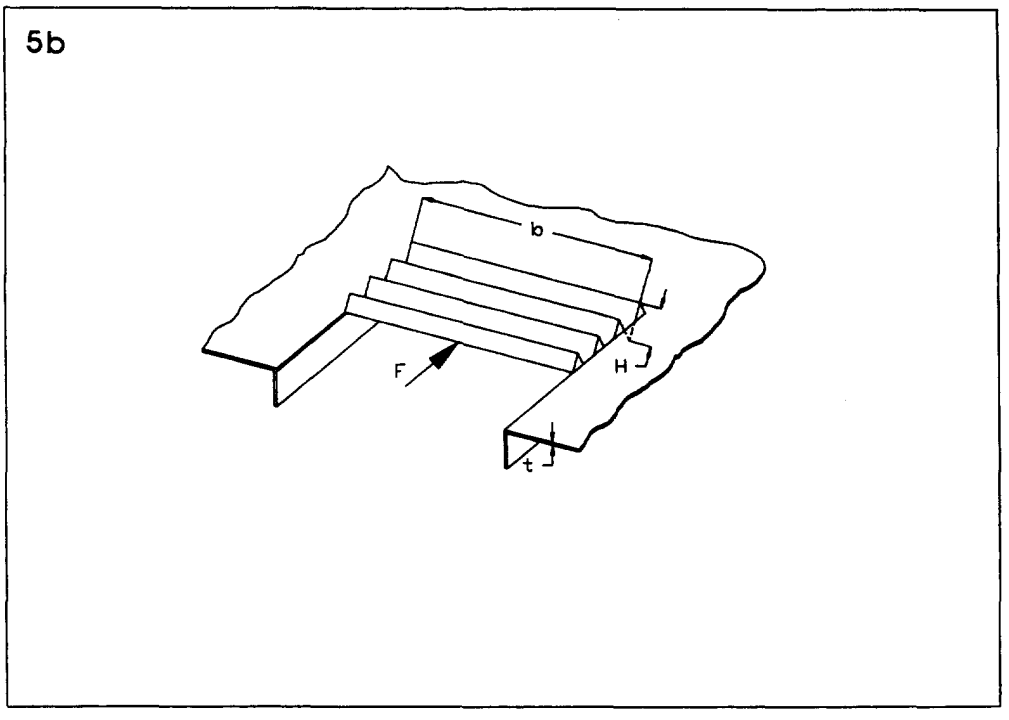

Fig. 5. Two conceptual models of concertina tearing. (a) Tearing of an infinite plate. (b) Tearing of a finite width plate with fully clamped longitudinal edge.

According to the present model, plastic deformation always spreads over two elements. Phase I of a given element corresponds to Phase II of the preceding element; Phase II of a given element corresponds to Phase I of the succeeding element. The present model describes a one-degree-of-freedom mechanism so that relative displacements and rotations of various plate elements can be easily determined and related to the displacement of the punch.

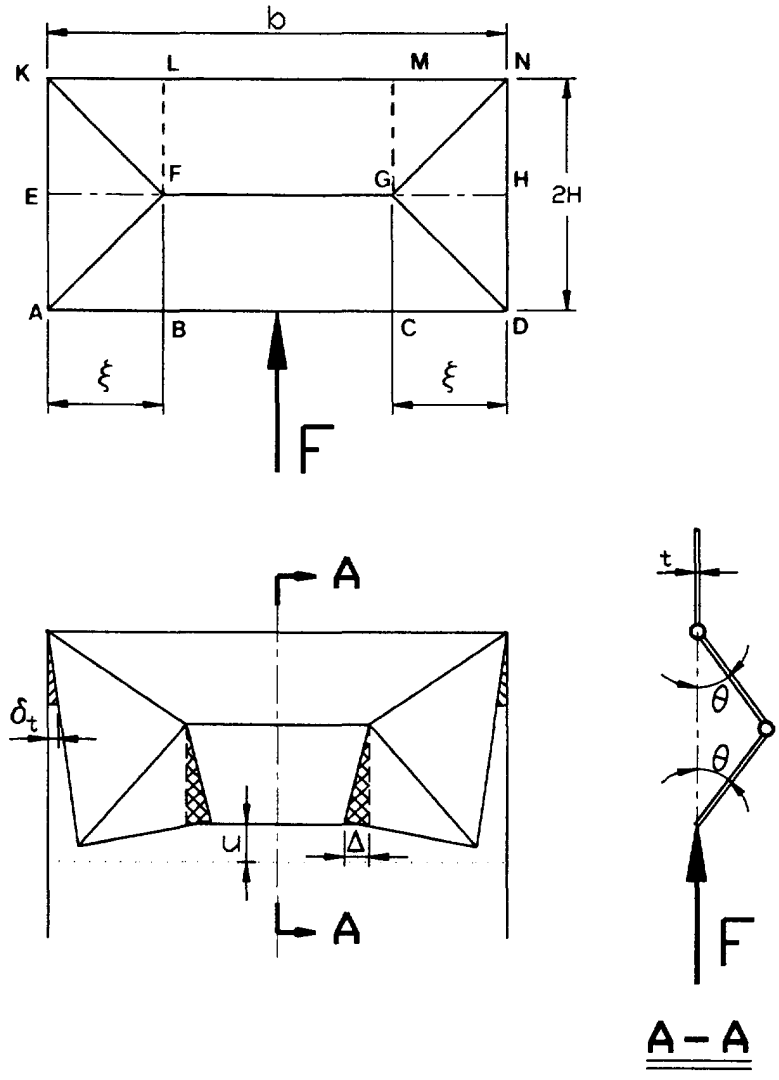

Fig. 7. Initial and current geometry (Phase I) of the deformed plate element under in-plane loading.

4. ASSUMPTIONS AND GOVERNING EQUATIONS

The concertina tearing problem involves combined plastic flow and fracture. Because plastic strains are two orders of magnitude larger than the elastic strains, the latter ones are neglected and a rigid-plastic material idealization is adopted. Accordingly, a two-parameter representation of the material properties will be used. The plastic flow is characterized by the flow stress σ_0, which is understood to be an elevated magnitude of stress corresponding to the average value of the strain in a given deformation region. An iterative procedure of calculating σ_0 from a known strain-hardening tensile characteristic of the material is described in Section 12. Following Atkins (1988), the tearing strength of the plate is characterized by a specific work of fracture R, which must be measured from separate experiments. Alternatively, R can be related to the flow stress and two new parameters:

$$R = m\sigma_0\delta_t, \tag{1}$$

where δ_t is the crack opening displacement (COD) parameter and m is a three-dimensionality factor.

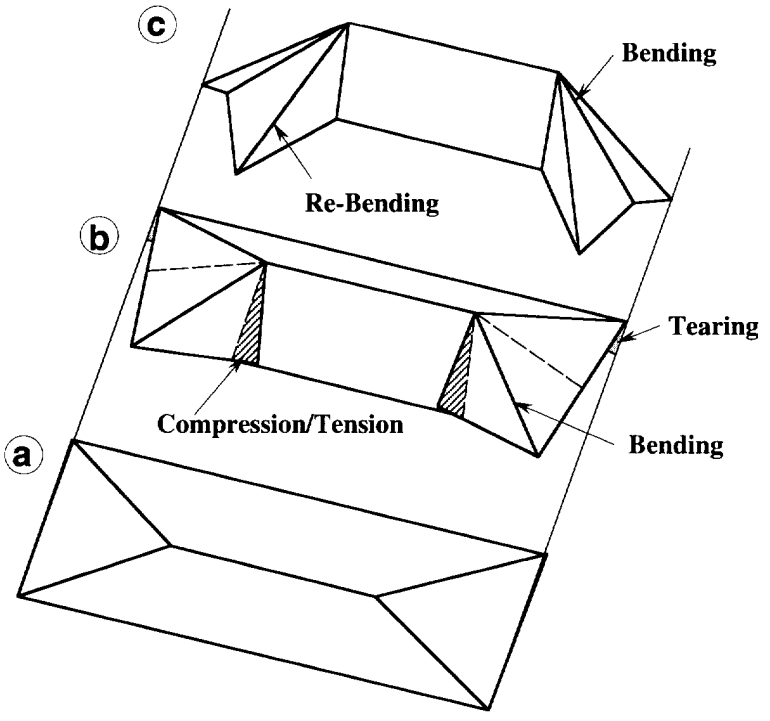

Fig. 8. A two stage computational model of concertina tearing. (a) Undeformed plate. (b) Bending, compression/tension and tearing. (c) Bending and rebending.

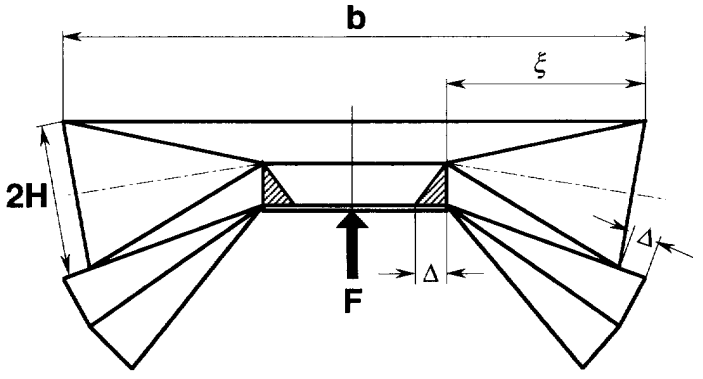

Fig. 9. Compatibility of two neighboring plate elements requires shear deformation to be developed along part of the boundary separating these elements.

As the wedge is pushed into the plate at a controlled constant speed $\dot{u}$, the driving force F, which produces the periodic concertina collapse of the plate, is obviously time-dependent. At any instant the power input is assumed to be related to the energy dissipation rate through the following equation:

$$F\dot{u} = \dot{E}_b + \dot{E}_m + \dot{E}_{sh} + \dot{E}_f, \tag{2}$$

where $\dot{E}_b$ is the rate at which energy is dissipated into plate bending. Likewise, $\dot{E}_m$, $\dot{E}_{sh}$ and $\dot{E}_f$ correspond to plate stretching (membrane action), plate shearing and plate fracture/tearing, respectively. Each of these energy dissipation rates vary differently with time. For the cyclic process being considered, the average value of F, denoted by F_m, is given by $F_m\Gamma = \int_0^\Gamma F\,dt$, where Γ is the period, i.e. the time taken for the wedge to advance a distance $2H$. Clearly, $\Gamma = 2H/\dot{u}$, where $2H$ is the characteristic concertina length, at present unknown. In view of the complicated time dependencies it is advantageous to consider the integrated form of (2):

Table 1. Contribution of bending deformation to the plate resisting force

Phase	Hinge	l_i	ϕ_i
Phase I	Edge	$2b$	$\pi/2$
	Central	$b-2\xi$	π
	Diagonal	4ξ	$\pi/2$
Phase II	Central	2ξ	π
	Diagonal	4ξ	$\pi/2$

$$F_m \dot{u}\Gamma = 2HF_m = \int_0^\Gamma \dot{E}_b \, dt + \int_0^\Gamma \dot{E}_m \, dt + \int_0^\Gamma \dot{E}_{sh} \, dt + \int_0^\Gamma \dot{E}_f \, dt \tag{3}$$

or

$$F_m = \frac{1}{2H}[E_b + E_m + E_{sh} + E_f], \tag{4}$$

where

$$E_b = \int_0^\Gamma \dot{E}_b \, dt.$$

5. ENERGY DISSIPATION DUE TO BENDING

According to the assumed kinematic model of the problem, all plastic bending is concentrated in a system of stationary hinge lines and no work is dissipated in the continuous bending mode. The rate of bending work in the ith hinge line is equal to the product of the fully plastic bending moment M_0, the rate of hinge rotation $\dot{\phi}_i$, and the length of the hinge line l_i:

$$(\dot{E}_b)_i = M_0 l_i \dot{\phi}_i. \tag{5}$$

Integrating eqn (5) in time and summing over all hinge lines gives:

$$E_b = M_0 \sum_i l_i \phi_i. \tag{6}$$

The length and total rotations in the first and second phases of the folding process are listed in Table 1 (refer to Fig. 7). Note that for simplicity the length of a diagonal hinge has been approximated by its projection in the transverse direction.

Substituting the values from Table 1 into eqn (6), the total bending energy becomes:

$$E_b = 2\pi M_0[b + 2\xi], \tag{7}$$

where

$$M_0 = \frac{1}{2\sqrt{3}} \sigma_0 t^2 \tag{8}$$

is the plain strain fully plastic bending moment per unit length. Note that the contribution of the hinge lines FL and GM of the total length $2H$ rotating by an angle arctan H/ξ is small compared to other terms and has been neglected in eqn (7).

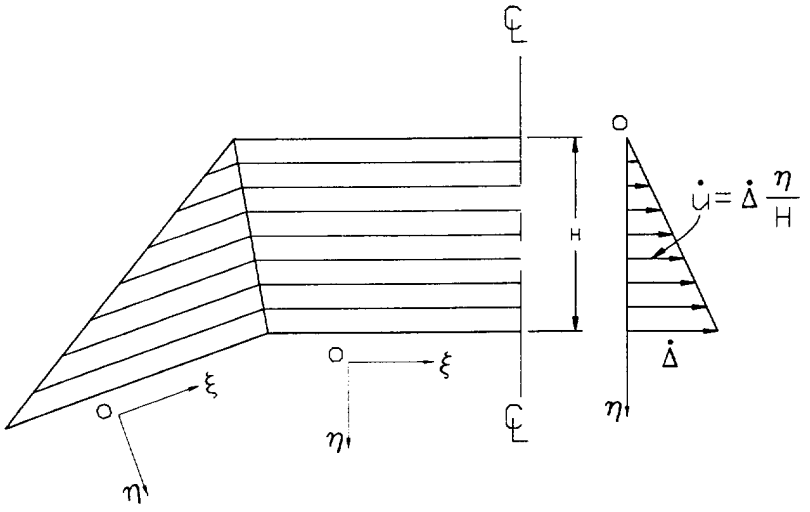

Fig. 10. A local coordinate system imbedded in the deforming trapezoidal element and the assumed linear velocity distribution.

6. ENERGY DISSIPATION DUE TO MEMBRANE ACTION

The rate of membrane work in the plane stress condition is

$$\dot{E}_{\mathrm{m}} = t \int_S \sigma_{\alpha\beta} \dot{\varepsilon}_{\alpha\beta} \, \mathrm{d}S, \quad \alpha, \beta = 1, 2, \tag{9}$$

where $\sigma_{\alpha\beta}$ and $\dot{\varepsilon}_{\alpha\beta}$ denote respectively components of the stress and strain rate tensor in the deformed configuration. According to the assumed kinematic model, the membrane deformations are confined to the front trapezoidal element (Fig. 8). The remaining trapezoidal and triangular elements rotate with respect to each other as rigid bodies. It is convenient to introduce a local coordinate system (ξ, η) which rotates with the deforming front trapezoid (Fig. 10). The so-called velocity strain is defined by

$$\dot{\varepsilon}_{\alpha\beta} = \tfrac{1}{2}(\dot{u}_{\alpha,\beta} + \dot{u}_{\beta,\alpha}), \quad \alpha, \beta = \xi, \eta, \tag{10}$$

where $\dot{u}_\alpha = (\dot{u}_\xi, \dot{u}_\eta)$ are components of the velocity vector in the local coordinate system which rotate with rigid trapezoidal or triangular elements. Because the plate buckles and folds in front of the wedge, it is assumed that the trapezoidal element is inextensible in the η direction, i.e. $\dot{u}_\eta = 0$ and $\dot{\varepsilon}_{\eta\eta} = 0$. The rate of shear work is neglected, $\sigma_{\xi\eta}\dot{\varepsilon}_{\xi\eta} = 0$, in the tension-dominant regions; conversely, the rate of tension work is neglected in the shear-dominant regions. The only non-vanishing component of the strain rate vector describes compression in the transverse direction, $\dot{\varepsilon}_{\xi\xi} = \partial \dot{u}_\xi / \partial \xi$. The present kinematic model suggests that plastic compression is confined to a local triangular zone marked in Figs 7 and 8 by a shaded area. The overlapping zones have been shaded only for illustrative purposes. In fact, plastic zones could extend at a finite distance $^{-}\xi(\eta)$; $^{+}\xi(\eta)$ on both sides of the generalized compression hinge. In the case of the Huber–Mises yield condition, the component of the stress tensor corresponding to $\dot{\varepsilon}_{\xi\xi}$ is $\sigma_{\xi\xi} = 2/\sqrt{3}\,\sigma_0$. The expression for the rate of membrane energy per one side reduces to

$$\dot{E}_{\mathrm{m}} = \frac{2}{\sqrt{3}} \sigma_0 t \int_0^H \int_{-\xi(\eta)}^{+\xi(\eta)} \frac{\partial \dot{u}_\xi}{\partial \xi} \, \mathrm{d}\xi \, \mathrm{d}\eta = \frac{2}{\sqrt{3}} \sigma_0 t \int_0^H \dot{u} \, \mathrm{d}\eta, \tag{11}$$

where $\dot{u}(\eta) = \dot{u}_\xi(^{+}\xi) - \dot{u}_\xi(^{-}\xi)$ is the relative transverse velocity between the left and right-hand sides of the trapezoidal element. In our model, this velocity is a linear function of the η-coordinate:

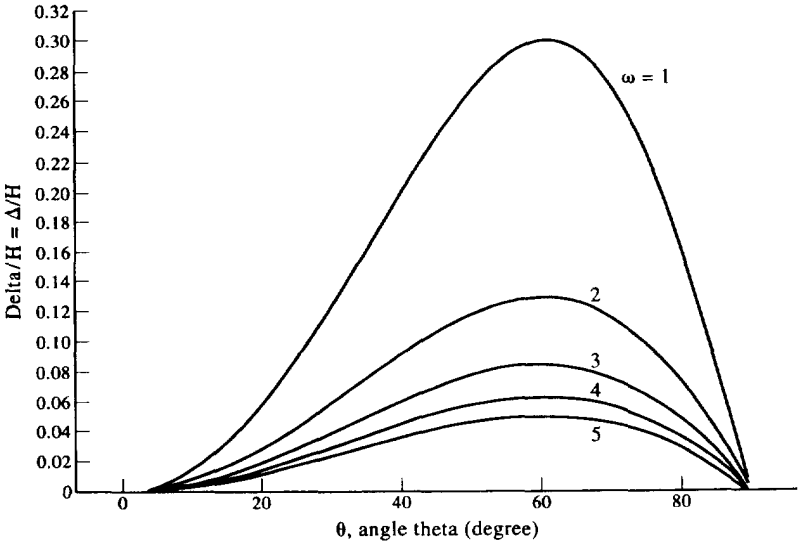

Fig. 11. A plot of the dimensionless amplitude of the transverse displacement versus the plate rotation angle for several values of the parameter ξ/H.

$$\dot{u}(\eta) = \dot{\Delta}\frac{\eta}{H}. \tag{12}$$

where $\dot{\Delta}$ is the maximum (tip) velocity difference at the transverse edge of the plate. Introducing eqn (12) into eqn (11) and integrating the latter yields

$$\dot{E}_m = \frac{1}{\sqrt{3}}\sigma_0 H\dot{\Delta}t. \tag{13}$$

The expression for the tip velocity $\dot{\Delta}$ as a function of H, ξ and the process parameter θ is derived in Appendix A. A plot of the dimensionless displacement Δ/H versus the process parameter θ for various values of ξ/H is shown in Fig. 11. The function Δ/H increases initially, reaches a maximum value Δ_{max}/H at $\theta^* = 60^\circ$, and then decreases back to zero. Therefore, the initial compression of the trapezoidal element for $0 < \theta < \theta^*$ gives rise to tension in the remainder of the process, $\theta^* < \theta < 90^\circ$. The strain reversal should be taken into account in integrating eqn (13) with respect to time:

$$E_m = \frac{2H}{\sqrt{3}}\Delta_{max}\sigma_0 t, \tag{14}$$

where an approximate expression for Δ_{max} (see Appendix A) is $\Delta_{max} = H^2/4\xi$. The final expression for the total plastic energy dissipation by the membrane action in two compression/tension regions is

$$E_m = \frac{1}{\sqrt{3}}\sigma_0\frac{H^2}{\xi}t. \tag{15}$$

7. ENERGY DISSIPATION DUE TO SHEAR

As described in Section 2, there is a relative shear displacement between the boundary of two subsequent folding elements. This displacement is assumed to produce uniform shear strains in the back rectangular element of the area $S = \xi H$ (the front trapezoidal element undergoes tension/compression). From eqn (9) the rate of shear energy per one side is

$$\dot{E}_{\mathrm{sh1}} = \frac{\sigma_0}{\sqrt{3}} t \int_S 2\dot{\varepsilon}_{\xi\eta}\, \mathrm{d}S. \tag{16}$$

Using eqns (9), (10) and (12), the expression for the shear energy per one side becomes

$$E_{\mathrm{sh1}} = \tfrac{1}{2} M_0 \frac{H^2}{t}. \tag{17}$$

This energy should be doubled because there are two identical elements on both sides of the symmetry line and doubled again because of the shear strain reversal.

8. ENERGY DISSIPATION DUE TO TEARING

The tearing process of thin plates has been discussed extensively by Atkins (1988). Stronge *et al.* (1983, 1984) performed an experimental and theoretical study on the problem of splitting of tubes and concluded that the relative contribution of the tearing energy to the total energy dissipation is small. In the present paper, estimates on the tearing energy will be made using the concept of a crack opening displacement (COD) parameter.

Progressive tearing along the longitudinal edges is precipitated by membrane straining in the transverse direction. Therefore, the energy of tearing can be regarded as a membrane energy up to the point of fracture. Neglecting, as before, the effect of shear, eqn (11), for the rate of membrane energy still applies where η is a coordinate along the edge of the plate and the integration extends over the whole length of the fold $[0, 2H]$. The energy of tearing fracture is obtained by integrating eqn (11) in time over the full loading cycle. At any material element η the cycle starts with zero displacement and terminates when the displacement reaches the critical value for fracture. This critical value is called the COD or the crack tip opening displacement (CTOD) parameter δ_t. The tearing energy is:

$$E_t = \int \dot{E}_m \, \mathrm{d}t = \frac{2}{\sqrt{3}} \sigma_0 t \int_0^{2H} \mathrm{d}\eta \int_0^{\delta_t} \mathrm{d}u = \frac{2}{\sqrt{3}} \sigma_0 t \delta_t 2H. \tag{18}$$

It was shown by Wierzbicki and Thomas (1993) that shear energy, neglected in the above first order estimate, is approximately equal to one half the tension energy. The energy of fracture (per tear), corrected for shear becomes [see eqn (1)]

$$(E_t)_{\mathrm{corr}} = 1.74 \sigma_0 \delta_t (2Ht) = 2HtR, \tag{19}$$

where, according to Atkins (1988), the three-dimensionality factor m appearing in eqn (1) is approximately $m = \sqrt{3}$ for plane stress states.

9. FOLDING WAVELENGTH

Substituting the expression for E_b, E_m, E_{sh} and E_t, calculated in Sections 6–8, into eqn (4), the dimensionless mean indentation force is given by

$$\frac{F_m}{M_0} = \pi \frac{b}{H} + 2\pi \frac{\xi}{H} + \frac{H^2}{\xi t} + 2\frac{H}{t} + 4\sqrt{3}\frac{R}{\sigma_0 t}, \tag{20}$$

where b, t and R are considered to be known. The mean indentation force is seen to depend on two parameters, H and ξ. Following the procedure used successfully in the crushing analysis of metal tubes (Alexander, 1960; Wierzbicki and Abramowicz, 1983), it is postulated that the unknown parameters adjust so as to minimize the mean indentation force

$$\frac{\partial F_m}{\partial H} = \frac{\partial F_m}{\partial \xi} = 0. \tag{21}$$

Attempts have recently been made to rationalize the above postulate for a class of steady-state and periodic plasticity problems (Abramowicz, 1994).

The extension of the minimum postulate, extensively verified in the literature dealing with crashworthiness calculations, to the case of combined flow and fracture is justified on the following grounds. The last term in eqn (20) represents the contribution to the indentation force due to fracture. However, this term depends neither on H nor on ξ. Therefore, the length of the plastic folding wave H must depend on a relative contribution of bending, shear and membrane energies, which was the case with previous applications of the minimum energy principle.

The condition (34) leads to two algebraic equations for H and ξ:

$$\frac{1}{t} + \frac{2H}{\xi t} - \frac{\pi}{H^2}(b+2\xi) = 0, \tag{22}$$

$$\frac{2\pi}{H} - \frac{H^2}{\xi^2 t} = 0,$$

whose approximate solution is:

$$\frac{H}{t} = \left(\frac{b}{t}\right)^{0.57} \tag{23}$$

$$\frac{\xi}{t} = 0.4\left(\frac{b}{t}\right)^{0.855}. \tag{24}$$

The wavelength H is seen to be independent of the mechanical properties of the material and is governed by the thickness of the plate and the width of the torn strip. In this respect there is a full analogy with the problem of axial crushing of circular square tubes [see Alexander (1960) and Wierzbicki and Abramowicz (1983)].

10. MEAN INDENTATION FORCE

Substituting the optimum values of the parameters H and ξ, given by eqns (23) and (24), into eqn (20), the expression for the mean indentation force can be put in a simple power form:

$$F_m = 3\sigma_0 t^{5/3} b^{1/3} + 2Rt. \tag{25}$$

Equation (25) was derived on the assumption that over one cycle the plate is shortened over the entire length of the folding wave $2H$. A cross-section through a folded part of the plate reveals that the "concertina" is composed of alternating circles rather than straight segments. The effective crush distance is thus smaller and equal to approximately 75% of the available crush distance. Therefore, eqn (4) for the work of external forces should be replaced by $E_{ext} = F_m \frac{3}{4}(2H) = F_m \frac{3}{2} H$ (Abramowicz, 1983). Accordingly, the expression for the mean indentation force should be increased by a factor of 4/3:

$$F_m = 4\sigma_0 t^{5/3} b^{1/3} + \frac{8}{3} Rt. \tag{26}$$

11. ALTERNATIVE SOLUTION

In Section 3 it was shown that at the interface of two folding elements there is a relative slide between the segment MN of a given element and the segment C′D′ of the next element. The magnitude of the slide was denoted by Δ and its maximum value was denoted by Δ_{max}. The corresponding plastic work dissipated in the shear hinge is given by eqn (17).

Another way of accommodating the relative displacement Δ would be to compress the triangle GMN in Phase II to make it compatible with the compression of the next element C′D′G′ in Phase I of the folding process. Such a formulation is not rigorous but leads to much simpler algebra. Now the shear contribution in the energy balance equation should be dropped while the membrane tension/compression energy should be doubled. Accordingly, eqn (20) is replaced by

$$\frac{F_m}{M_0} = \pi \frac{b}{H} + 2\pi \frac{\xi}{H} + 2\frac{H^2}{\xi t}. \tag{27}$$

The above mean indentation force F_m has a simple analytical minimum with respect to the parameters H and ξ, which occurs at

$$\xi = b/6 \tag{28}$$

$$H = \left(\frac{\pi}{18}\right)^{1/3} b^{2/3} t^{1/3} = 0.56 b^{2/3} t^{1/3}. \tag{29}$$

The corresponding optimum value of F_m is

$$F_m = 3.25\sigma_0 t^{5/3} b^{1/3} + 2Rt. \tag{30}$$

This is an identical result to eqn (25) except for a different (8% higher) coefficient in the first term corresponding to plastic energy dissipation. The final expression for the mean indentation force, corrected by the effective crush distance, is

$$F_m = 4.33\sigma_0 t^{5/3} b^{1/3} + \tfrac{8}{3} Rt. \tag{31}$$

12. EFFECT OF STRAIN-HARDENING

The material constant σ_0 in the present computational model is understood as the elevated value of the flow stress corresponding to the average value of strain ε_{av} in the loading process. If the stress–strain diagram of a given material is described by the function $\sigma = f(\varepsilon)$, then

$$\sigma_0 = f(\varepsilon_{av}). \tag{32}$$

Usually, the flow stress settles somewhere between the initial yield stress and the ultimate stress of the material $\sigma_y < \sigma_0 < \sigma_u$. Strains obtained in various deformation zones are, in general, different. Assuming that tensile strains are uniformly distributed over the width of the plate, the average membrane strain ε_{av}^m is defined by

$$\varepsilon_{av}^m = \frac{\Delta_{max}}{b}. \tag{33}$$

Using eqns. (A.4), (28) and (29), the expression for the average membrane strain becomes

Table 2. Comparison of measured and predicated fold lengths

Test #	t [mm]	$(2H)$th, eqn (38) [mm]	$(2H)$ exp [mm]	% Difference
1	0.749	46.02	38.42	16.5†
5	1.143	55.20	50.80	7.9
6	0.7366	45.69	39.69	13.1
7	0.7366	45.69	39.01	14.6‡
9	0.7366	45.69	39.01	14.6
10	0.7366	45.69	40.22	11.9
14	1.143	55.20	38.10	30.1†
15	0.7366	45.69	43.57	4.6
16	1.143	55.20	51.71	6.3

†Frame tilt angle $\alpha = 10$
‡Frame tilt angle $\alpha = 40$

$$\varepsilon_{av}^{m} = 1.45\left(\frac{t}{b}\right)^{2/3}. \tag{34}$$

According to the Love–Kirchhoff hypothesis, the strains are linearly distributed across the plate thickness. The average bending strain ε_{av}^{b} in the concentrated fold zones is

$$\varepsilon_{av}^{b} = \frac{t}{4r}, \tag{35}$$

where r is the local radius of curvature of the fold. The radius of cylindrical bending depends on the length of the plate strip H and to a much lesser extent on the strain-hardening modulus. An approximate expression for the bending radius, derived by Abramowicz (1983), is $r = 0.28H$. Using eqns (29) and (35), the average bending strain becomes

$$\varepsilon_{av}^{b} = 1.59\left(\frac{t}{b}\right)^{2/3}. \tag{36}$$

On comparing eqns (34) and (36), one can see that the expressions for the average plastic strain are almost identical in the tension and bending zones. For convenience and simplicity we take the average value:

$$\varepsilon_{av} = 1.52\left(\frac{t}{b}\right)^{2/3}. \tag{37}$$

For plates with aspect ratios $50 < b/t < 200$, the average plastic strain is in the range $0.05 < \varepsilon_{av} < 0.12$.

13. COMPARISON WITH TESTS

The present theoretical solution will now be compared with two sets of experiments.

Correlation with wide plate tests

Maxwell (1983) performed 19 wedge indentation tests on plates with $b = 304.8$ mm for four different thicknesses. Of these, nine specimens failed in the concertina folding mode while the remaining 10 developed the central separation mode. Three specimens, nos 1, 7 and 14, experiencing concertina tearing were tested using a tilt angle of the apparatus. A comparison of measured and predicted fold lengths is shown in Table 2.

The large discrepancy in test nos 1, 7 and 14 can be explained by a frame tilt angle α, which is not accounted for by the present theory. There is also an obvious trend towards

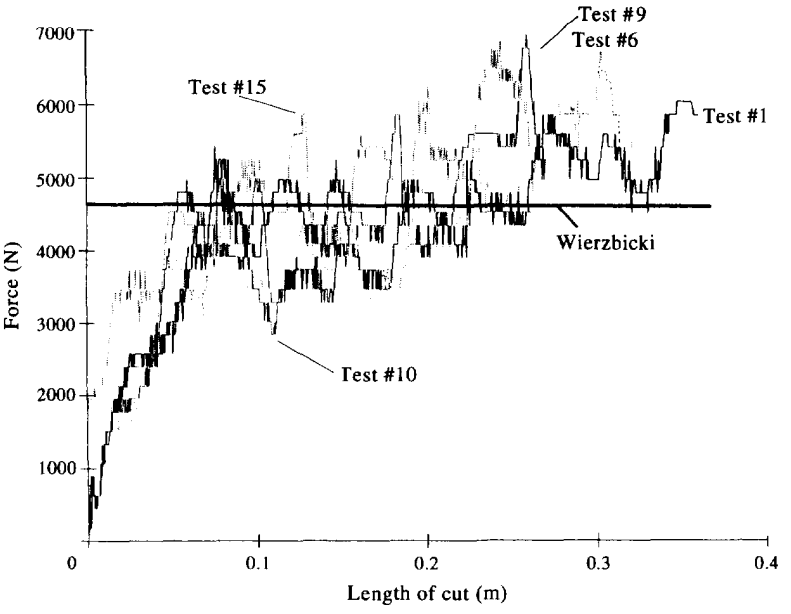

Fig. 13. Comparison of five indentation tests in the concertina folding mode with the theoretical solutions. Plate thickness $t = 0.74$ mm.

better correlation as the bluntness of the wedge increases. Test nos 15 and 16, for which the error in the predicted folding wavelength is the smallest, were conducted with a large diameter round wedge (Fig. 12). In the remaining tests the wedge was quite narrow, allowing the plate elements to rotate upwards and partially skip the second phase of folding (see, for example, Fig. 2). Clearly, a clean two-phase deformation process, which was the basis of the present computational model, was not achieved in the experiments.

A comparison of the theoretical mean indentation force with the experimentally measured force–displacement relation is shown in Fig. 13. In this figure, results of five tests on plates with nearly identical thicknesses are superimposed. Local peaks and valleys in individual curves correspond to the formation of subsequent folds. The horizontal line in Fig. 13 represents the present theoretical solutions. Taking the following values for the material and geometrical parameters,

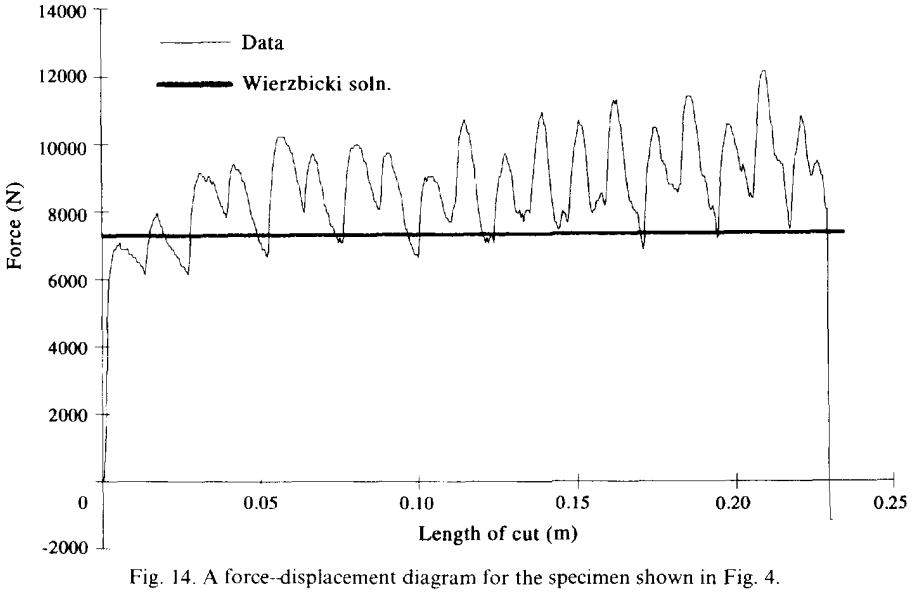

Fig. 14. A force–displacement diagram for the specimen shown in Fig. 4.

$$\sigma_0 = 250\ \text{N mm}^{-2},$$

$$R = 300\ \text{N mm}^{-1},$$

$$t = 0.74\ \text{mm and}$$

$$b = 304.8\ \text{mm},$$

eqn (26) for the mean indentation force gives $F_m = 4665$ N. The agreement is very good considering the complexity of the problem. The flow stress was measured from the hardness tests, which give the stress corresponding to 8% strain. The specific work of fracture was estimated (Atkins, 1988) but the dependence of the solution on the parameter R is rather weak.

Correlation with narrow plate tests

The second set of tests, performed by Yahiaoui *et al.* (1994), was better controlled and corresponds much more closely to the present computational model. The process of concertina tearing was activated by a right angle wedge on a long and narrow plate strip. The plate strip was isolated from the previously used plates mounted on a U-frame by two longitudinal stiffeners. The stiffeners were welded to the plate by an electron beam technique at a distance $b = 50$ mm apart. A photograph of the damaged specimen, shown in Fig. 4, reveals an absolute regularity of the folding process. Tearing occurred along the stiffeners in a stable way. This regularity is also reflected in the recorded force–displacement curve (Fig. 14). Apart from the initial rise, the force level oscillates around an experimental average of approximately $(F_m)_{exp} \cong 8500$ N.

The plates were of thickness $t = 1.143$ mm, giving the aspect ratio $b/t = 43.74$. The resulting average strain calculated from eqn (37) is $\varepsilon_{av} = 0.12$. The stress–strain curve was carefully measured on a coupon cut-out from the plate, and the flow stress corresponding to 12% strain was found to be $\sigma_0 = 330$ N mm^{-2}. Using the above values and an estimated specific work of fracture $R = 300$ N mm^{-1}, the theoretical mean indentation force calculated for the second round of tests from eqn (26) is $F_m = 6760$ N. A better prediction is obtained from the alternative solution [eqn (31)], $F_m = 7323$ N, with a resulting error of 13.8%.

In Fig. 4, one can distinguish 19 distinct peaks which are typically $2H$ apart. The total measured length of the torn part of the plate is $l = 280$ mm. The length of the folding wave measured from the test is $H_{exp} = 280/38 = 7.37$ mm. At the same time the folding wavelength predicted by eqn (23) is $H_{th} = 7.87$ mm, which is only 6.3% in error.

14. DISCUSSION AND CONCLUSION

A closed-form solution was derived for the mean indentation force and the length of the folding wave in the process of "concertina tearing" of ductile metal plates. The present computational model captures all of the main features of the deformation process, such as in-plane tearing, out-of-plane folding, interaction of two subsequent folding waves and strain reversal. A comprehensive test program was undertaken for mild steel plates with a wide range of width to thickness ratios to validate the theory. The accuracy achieved in predicting the mean indentation force and the folding wavelength was typically in the range 5–15%. The correlation between the theory and experiment is good considering the complexity of the physical problem and the simplicity of the computational model. The present solution is based on the concept of stationary tension/compression, shear and bending hinge lines with slope discontinuities and rigidly displacing and rotating plate elements. The present model can be further improved by smoothing out bending deformations over a finite width, introducing moving hinge lines and spreading deformation over more than two folds. This will add complexity to the solution with some improvements in the accuracy.

There is a great deal of similarity between the problem of axial crushing of square or rectangular tubes and the present problem of concertina tearing. For example, the fractional powers in the expression for H and F_m are in both cases identical, and the only difference

is in the numerical coefficient [see Wierzbicki and Abramowicz (1983)]. The fracture process is important in that it induces a certain deformation mode and provides a mechanism of clearing the plate material in the out-of-plane mode from the path of the indentor. The relative contribution of plastic deformation and fracture to the mean indentation force can be determined from eqn (30). For example, taking the material parameters of the present narrow plate experiments, the ratio of plastic to fracture resistance is of the order of 10% over a wide range of b/t. This is in accord with earlier results of Stronge *et al.* (1983, 1984) concerning splitting of tubes.

There are further interesting features of the present solution. In the previous analysis of the wedge cutting problem, the plate resistance was shown to depend on the wedge semi-angle θ, the wedge tip radius r and the friction coefficient μ (Wierzbicki and Thomas, 1993; Lu and Calladine, 1990). None of the above parameters enter the present solution because the material piles up in front of the wedge rather than curls and contacts the wedge in the wake of the crack tip.

Finally, it should be noted that the present solution applies when tearing proceeds along a clamped boundary of the plate. An explanation of why the tear remains at the boundary in a finite plate and a prediction of the crack trajectory in an infinite plate initiating from a local cut can be found in a separate publication (Wierzbicki and Trauth, 1995).

Acknowledgements—The work presented herein was supported by the Joint MIT–Industry Consortium on Tanker Safety and by the Contract no. N00167-93-K-0014 from the Naval Surface Warface Center. The author would like to express his appreciation to Frank McClintock and Tony Atkins for discussing various aspects of the present formulations. Thanks are also due to K. Trauth and M. Yahiaoui for helping in the experimental part of the paper, to Zi-Ming Zheng for performing calculations presented in the Appendix and to M. Sinmao for helping in the preparation of the manuscript.

REFERENCES

Abramowicz, W. (1983). The effective crushing distance in axially compressed thin-walled metal columns. *Int. J. Impact Engng* **1**, 309–317.

Abramowicz, W. (1994). Private communication.

Alexander, J. M. (1960). An approximate analysis of the collapse of thin cylindrical shell under axial loading. *Q. J. Mech. Appl. Math.* **13**, No. 1, 10–15.

Astrup, O. (1994). Cutting of thick plates by a wedge—an experiment study. Report No. 27, Joint MIT–Industry Program on Tanker Study.

Atkins, A. G. (1988). Scaling in combined plastic flow and fracture. *Int. J. Mech. Sci.* **30**, 173.

Jones, N. and Jouri, W. S. (1987). A study of plate tearing for ship collision and ground damage. *J. Ship Res.* **31**, 253.

Kitamura, K., Okumoto, Y. and Shibue, T. (1978). On the model tests of double bottom strength for stranding (in Japanese). *J. Soc. Naval Architects Japan* **143**, 346–356.

Kuroiwa, T., Kawamoto, Y. and Yuhara, T. (1992). Study on damage of ship bottom structures due to grounding. *Proc. Conf. on Prediction Methodology of Tanker Structural Failure*, Tokyo, Japan.

Lu, G. and Calladine, C. R. (1990). On the cutting of a plate by a wedge. *Int. J. Mech. Sci.* **32**, 295–313.

Maxwell, L. M. (1993). Effect of rock geometry in the failure mode of plates and the forces in grounding experiments. M.S. Thesis, Department of Ocean Engineering, MIT. Also Report No. 15, Joint MIT-Industry Program on Tanker Safety.

Paik, J. K. (1994). Cutting of a longitudinally stiffened steel plate by a rigid wedge. Submitted to *J. Ship Res.*

Stronge, W. J., Yu T. X. and Johnson, W. (1983). Long stroke energy dissipation in splitting tubes. *Int. J. Mech. Sci.* **25**, 637–647.

Stronge, W. J., Yu T. X. and Johnson, W. (1984). Energy dissipation by splitting and curling tube. In *Structural Impact and Crashworthiness* (Edited by J. Morton), Vol. 2, pp. 576–587. Applied Science, London.

Thomas, P. (1992). Application of plate cutting mechanics to damage prediction in ship groundings. Report No. 8, Joint MIT–Industry Program on Tanker Safety.

Vaughan, H. (1979). The tearing and cutting of mild steel plate with application to ship grounding damage. *Proc. 3rd Int. Conf. Mechanical Behavior of Materials* (Edited by K. F. Miller and R. F. Smith), Vol. 3, pp. 479–487. Pergamon Press, Oxford.

Wierzbicki T. and Abramowicz, W. (1983). On the crushing mechanics of thin walled structures. *J. Appl. Mech.* **5**, 727–734.

Wierzbicki, T., Bhat, S. U., Abramowicz, W. and Brodkin, D. (1992). Alexander revisited—a two folding elements model of progressive crushing of tubes. *Int. J. Solids Structures* **29**, 3269–3288.

Wierzbicki, T. and Huang, J. (1991). Initiation of plastic folding mechanisms in crushed box columns. *Thin Walled Structures* **13**, 115–143.

Wierzbicki, T., and Thomas, P. (1993). Closed-form solution for wedge cutting force through thin metal sheets. *Int. J. Mech. Sci.* **35**, No. 4, 209–229.

Wierzbicki, T. and Trauth, K. (1995). Concertina tearing of an infinite plate initiating from a local cut. Submitted to *J. Appl. Mech.*

Yahiaoui, M., Bracco, M., Little, P. and Trauth, K. (1994). Experimental studies on scale models for grounding. Report No. 19, Joint MIT–Industry Program on Tanker Safety.

APPENDIX

Calculation of the overlay function Δ

The dimensionless function Δ/H can be calculated from the geometry of the deforming prism, shown in Fig. 7

$$\frac{\Delta}{H} = \frac{\omega - \cos\theta\sqrt{\omega^2 - \sin^2\theta}}{\omega^2 + \cos^2\theta} - \cos\theta, \tag{A.1}$$

where $\omega = \xi/H$ is the dimensionless attitude of the triangular element. The dependence of the function Δ/H on the process parameter θ for several values of ω is shown in Fig. 10. The function Δ/H is seen to attain a maximum at $\theta = 60°$ for all considered values of the parameter ω from the range $1 < \omega < 5$. Therefore, the maximum amplitude of the overlap is obtained from eqn (A.1) by setting $\theta = 60$

$$\frac{\Delta_{\max}}{H} = 0.5\frac{\omega - 0.5\sqrt{\omega^2 - 0.75}}{\omega^2 + 0.25}. \tag{A.2}$$

The above equation can be further simplified by assuming that ω^2 is much larger than unity

$$\frac{\Delta_{\max}}{H} \cong 0.25\frac{1}{\omega}. \tag{A.3}$$

Thus, an approximate expression for the maximum overlap is

$$\Delta_{\max} = 0.25\frac{H^2}{\xi}. \tag{A.4}$$

The above expression is used in the derivation of the membrane energy.